



Mesoporous microspheres composed of carbon-coated TiO₂ nanocrystals with exposed {0 0 1} facets for improved visible light photocatalytic activity

Beibei Li, Zongbin Zhao*, Feng Gao, Xuzhen Wang, Jieshan Qiu*

Carbon Research Laboratory, Liaoning Key Lab for Energy Materials and Chemical Engineering, State Key Lab of Fine Chemicals, Dalian University of Technology, Dalian 116023, China

ARTICLE INFO

Article history:

Received 2 August 2013

Received in revised form 9 October 2013

Accepted 12 October 2013

Available online 18 October 2013

Keywords:

Anatase with active facets

Assembly

Carbon deposition

Visible light photocatalytic activity

ABSTRACT

Mesoporous TiO₂ microspheres composed of carbon-coated anatase nanocrystals with exposed {0 0 1} facets (TiO₂(0 0 1)/C) have been successfully synthesized by a one-pot hydrothermal strategy in the presence of glucose and hydrofluoric acid (HF). It is demonstrated that the presence of HF promotes the growth of anatase nanocrystal with {0 0 1} facet exposure, while glucose induces TiO₂ {0 0 1} nanocrystals to assemble into mesoporous TiO₂ microspheres, as well as acts as carbon source in the formation of carbonaceous layer deposited on the TiO₂ grains via C–O–Ti bond. The TiO₂(0 0 1)/C microspheres show an excellent visible-light driven photocatalytic performance for the degradation of methyl blue. These results provide insight into the preparation, assembly and modification of TiO₂ nanocrystals with active facets for potential application in environment protection.

© 2013 Elsevier B.V. All rights reserved.

1. Introduction

Anatase titanium dioxide (TiO₂) has been widely studied due to its excellent photocatalytic activity and potential applications towards photo-splitting of water, photocatalysis, photonic devices, and sensors [1–4]. The photocatalytic performance of TiO₂ is strongly dependent on its crystal structure, size and shape [4]. In recent years, lots of efforts have been devoted to control the exposed facets of TiO₂ crystals for their photocatalytic activity improvement [5–7]. Both theoretical and experimental studies of anatase TiO₂ indicated that the {0 0 1} facets are much more reactive than the {1 0 1} facets [6,8,9]. However, the surface energy for the {0 0 1} facets of anatase TiO₂ (0.90 J m^{-2}) is two times higher than that of the {1 0 1} facets (0.44 J m^{-2}). As a result, the {0 0 1} facets usually diminish rapidly during the anatase crystal growth process to minimize the surface energy, which leads to the surface of the product dominated with the less reactive {1 0 1} facets [10]. An important breakthrough in preparation of anatase TiO₂ single crystals with exposed {0 0 1} facets was achieved by Yang and his colleagues [11], who selected hydrofluoric acid (HF) as a shape controlling agent to synthesize micro-sized single crystallites of anatase TiO₂ with 47% {0 0 1} facets. Following this work, tremendous studies have been carried out to fabricate single anatase TiO₂

with much smaller size, larger percentage of {0 0 1} facet exposing and higher photocatalytic activities [12–16].

Nevertheless, most of these TiO₂ products can be excited only under UV light irradiation, which accounts for about 5% of the solar spectrum. To enhance the effective utilization and conversion of solar energy, there are many groups attempting to extend the photoresponse of TiO₂ nanocrystals with exposed {0 0 1} or {1 0 1} facets to the visible-light via doping [17–24], deposition [25] and sensitization [26,27]. Very recently, because of the wider visible light absorbance, functional carbonaceous materials were chosen to couple with TiO₂ as a visible light sensitizer via C–O–Ti bond, which could be a promising strategy to improve the photocatalytic activities of TiO₂ under visible light [25,28–31]. Zhang and coworkers [25] reported the synthesis of visible light responsive graphite-like carbon deposited anatase TiO₂ single crystals with exposed {0 0 1} facets via the dehydration of glucose during the process of hydrothermal treatment. The loading of the graphite-like carbon layers gives rise to enhanced visible photocatalytic activity of TiO₂ nanosheets with exposed {0 0 1} facets for methyl orange (MO) degradation. Inagaki [32] has pointed out that the carbon-coating could both improve the performance of photocatalysts and modify their structures to give sensitivity for visible light. However, the practical application of these TiO₂ nanocarystals is usually limited due to their low surface areas and the difficulty for separation. It is desirable to construct a new structure composing of anatase TiO₂ materials with dominant {0 0 1} facets that offers both large surface area and good recyclability.

* Corresponding authors.

E-mail addresses: zbzhao@dlut.edu.cn (Z. Zhao), Jqiu@dlut.edu.cn (J. Qiu).

Spherical-like TiO_2 has been explored owing to the unique optical properties and ease of recovery in practical applications [33–39]. Thus, increasing attention has focused on developing the TiO_2 microspheres produced from nanocrystals with high percentage of reactive {001} facets through a simple solvothermal synthesis in the presence of HF or ammonium fluoride (NH_4F) as a shape controlling agent [40–45]. However, the construction of visible light responsive hierarchical spherical-like structures from these interesting anatase TiO_2 nanocrystals exposed with reactive {001} facets has not been realized.

In this work, we report a facile and one-step glucose-mediated hydrothermal route with the assistance of HF as crystal facet-capping agent for the preparation of mesoporous microspheres consisting of carbon-coated TiO_2 nanocrystals with exposed {001} facets ($\text{TiO}_2(001)/\text{C}$). The carbonaceous materials were formed on the surface of the TiO_2 crystals via the dehydration of glucose during the hydrothermal process. The chemical state of the carbonaceous species were studied and the as-prepared carbonaceous- TiO_2 composite exhibited enhanced photocatalytic activity for the decomposition of methyl blue (MB) under visible light irradiation.

2. Experimental methods

2.1. Preparation of sample

Hierarchical $\text{TiO}_2(001)/\text{C}$ microspheres consisting of anatase TiO_2 nanocrystals with abundant {001} facets were prepared via hydrothermal reaction. In a typical procedure, 1 g glucose was dissolved into 30 ml of distilled water and stirred for 30 min, then 2 ml Ti(OBu)_4 (TNB) was added dropwise to glucose solution slowly under vigorous stirring, white suspension was obtained. After stirring for 30 min, 0.235 ml hydrofluoric acid (with a concentration 40 wt%) was mixed with the white suspension. The resulting suspension was stirred for another 10 min and then transferred into Teflon-lined autoclave, followed by hydrothermal treatment at 180 °C for 12 h. After the autoclave was cooled naturally in air, a brown precipitate TiO_2/C was obtained, washed with distilled water and absolute ethanol for several times and then dried in vacuum at 80 °C for 10 h. For comparison, $\text{TiO}_2(101)/\text{C}$ microspheres were fabricated according to the same procedure except in the absence of HF. In addition, nano-sized TiO_2 (001) particles were produced in the same hydrothermal conditions without the presence of glucose. $\text{TiO}_2(001)$ microspheres were obtained by calcination of $\text{TiO}_2(001)/\text{C}$ microspheres in air at 550 °C for 5 h to remove the glucose derived carbonaceous species.

2.2. Catalyst characterization

The morphology was examined by field emission scanning electron microscope (FESEM, Hitachi S4800) and transmission electron microscopy (TEM, Philips Tecnai G220). X-ray diffraction (XRD) analysis of the prepared samples was carried out at room temperature with a Rigaku D/Max-2400X apparatus using $\text{Cu K}\alpha$ radiation, operated at 40 kV and 100 mA. Fourier transform-infrared (FT-IR) spectra were recorded on a Jasco FT/IR-430 spectrometer. Brunauer–Emmett–Teller surface areas (S_{BET}) and pore size distribution were obtained on a Micromeritics ASAP 2020 nitrogen adsorption apparatus. The sample was degassed at 200 °C for 5 h prior to measurements. Pore size distribution was calculated from desorption branches of isotherms by Barrett–Joyner–Halenda (BJH) method. Estimation of carbon content in the TiO_2/C composites were conducted by using thermo-gravimetric (TG, Diamond–Pyris) analysis. TG experiments were done by heating the sample in air from room temperature to 800 °C at a rate of 10 °C min⁻¹. The chemical composition was analyzed by X-rays photoelectron

spectroscopy with Al $K\alpha$ X-rays radiation (XPS, Thermo ESCALAB 250). The UV-vis diffuse reflectance spectra measurement was carried out on a Jasco V-550 spectrophotometer, using BaSO_4 as the reference sample.

2.3. Evaluation of photocatalytic activity

Photocatalytic degradation of methyl blue (MB) aqueous solution was chosen as the probe reaction to evaluate the activity of the prepared samples and all the experiments were performed at room temperature. Prior to the light irradiation, 0.01 g photocatalyst was put into a 50 ml quartz photo-reactor that contained 40 ml aqueous MB solution (10 mg L⁻¹). The mixture was stirred in the dark for 60 min to obtain the equilibrium adsorption–desorption state. A 250 W metal halogen lamp of which the UV light portion was filtered by a 2.0 M NaNO_2 solution was used as visible light source. During the irradiation, 4 ml sample suspension was taken out from the mixture at certain time intervals and immediately centrifuged. The concentration of the MB aliquots was examined using a UV-vis spectrophotometer (TU1810, Beijing Purkinje General Instrument Co. Ltd) at 664 nm. Moreover, for comparison, a 100 W high-pressure Hg lamp for which the strongest emission wavelength is 365 nm was used as the UV light source to evaluate the photocatalytic activities of as-prepared TiO_2/C composites and pure TiO_2 materials under UV light irradiation with other conditions the same as visible light irradiation.

3. Results and discussion

3.1. Morphology and crystal structure

The morphology of as-prepared samples was characterized by FESEM (Fig. 1). Microspheres with diameter 0.4–0.5 μm were formed in large scale during the hydrothermal process, as shown in Fig. 1a. Clearly, these spheres are actually consisted of enormous nanoparticles (Fig. 1b). However, TiO_2 nanoparticles rather than microspheres were observed in the absence of glucose (Fig. S1a). Therefore, it can be concluded that glucose acts as a morphological controller to direct the self-organization of nano-sized TiO_2 particles into a spherical structure.

The hierarchical spherical structures were further characterized by TEM, as shown in Fig. 2. As seen, TEM image also identified that the $\text{TiO}_2(001)/\text{C}$ spheres were assembled with nanoparticles. Fig. 2b showed a typical image of the enlarged fringe of a single sphere. The size of the TiO_2 nanocrystallites was quite uniform and was estimated to be around 15–20 nm, which is consistent with the SEM observation shown in Fig. 1b. It is interesting to find that these TiO_2 nanocrystals were featured by the laterally-viewed hexagonal shape and top-viewed square shape of truncated octahedra. According to the symmetries of anatase TiO_2 crystals as shown in Fig. 2c, the two flat square surfaces and the eight isosceles trapezoidal surfaces should be {001} facets and {101} facets, respectively. The same results could be also observed for pure TiO_2 particles prepared in the absence of glucose, as shown in Fig. S1b. The interfacial angle between the truncated facet and the surrounding facet is 68°, which can be attributed to the angle between the {001} and {101} facets of anatase [10]. Moreover, the high-resolution TEM image in Fig. 2d clearly shows that the fringe spacing of 0.35 nm corresponds to the {101} planes, while the fringe spacing of 0.235 nm corresponds to the {001} planes [12].

As for $\text{TiO}_2(101)/\text{C}$ microspheres (Fig. S1c and d), which were obtained in the absence of crystal facet-controlling agent HF, a plenty of aggregates of smaller particles (less than 5 nm in size) were packed together, which suggests the glucose which undergo

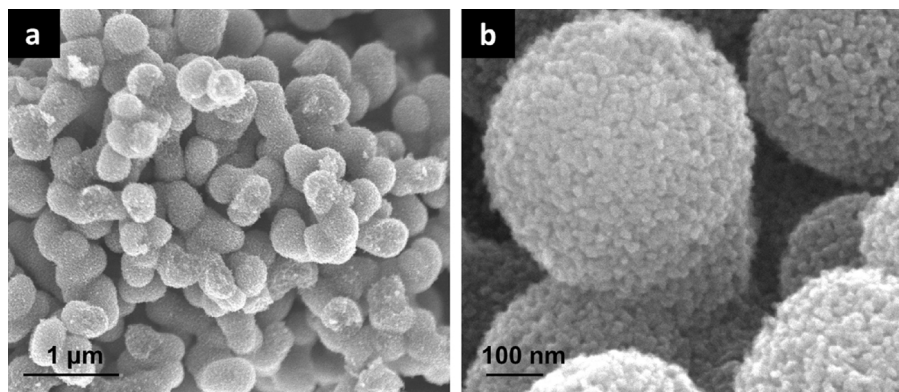


Fig. 1. (a) Low-magnification and (b) high-magnification FESEM images of mesoporous $\text{TiO}_2(001)/\text{C}$ spheres.

the dehydration, polymerization and carbonization process during hydrothermal conditions significantly affects the size and assembly of TiO_2 crystals, while HF could promote the growth of TiO_2 crystals with exposed $\{001\}$ facets [11].

Based on the above results, the proposed formation mechanism for the synthesis of mesoporous $\text{TiO}_2(001)/\text{C}$ microspheres was depicted in **Scheme 1**. During the hydrothermal process, (i) the presence of HF facilitates the conversion of Ti(OBu)_4 into TiO_2 nanocrystals exposed with $\{001\}$ facets. (ii) Carbonaceous spheres were derived from the dehydration and subsequent polycondensation of glucose molecules and the TiO_2 nanocrystals simultaneously integrated into the carbonaceous spheres. (iii) The growth of the carbonaceous microsphere and the continuous integration of newly formed TiO_2 nanocrystals exposed with $\{001\}$ during the hydrothermal process [27,42], forming a “mud and brick structure” [30,46].

After removal of the carbon layer in $\text{TiO}_2(001)/\text{C}$ microspheres by calcination in air, the spherical morphology remains, as shown in

Fig. S2. The high magnification TEM image (Fig. S2) evidences that the carbonaceous species coated on the TiO_2 grains were removed by calcination. It is obviously to find that the thermal calcination can generates pores ($\sim 2 \text{ nm}$) on both $\{001\}$ and $\{101\}$ facets of TiO_2 nanocrystals. Very recently, Pan and coworkers [47] reported that the escape of surface-capping F ions during the calcination process could give rise to the pore-forming, but the mechanism is still unclear.

Fig. 3 shows the XRD patterns of the TiO_2 samples obtained under different reaction condition. All the peaks of the resultant samples from hydrothermal reaction at 180°C can be indexed to the anatase phase of TiO_2 (JCPDS file No. 21-1272). The peaks of carbon are not observed in XRD patterns of the composites, which suggest the presence of carbonaceous materials rather than crystalline carbon in these composites. The diffraction peaks of $\text{TiO}_2(101)/\text{C}$ synthesized in the absence of hydrofluoric acid are considerably broad, which may be attributed to the small size of the TiO_2 crystallites, consistently with TEM characterization mentioned above.

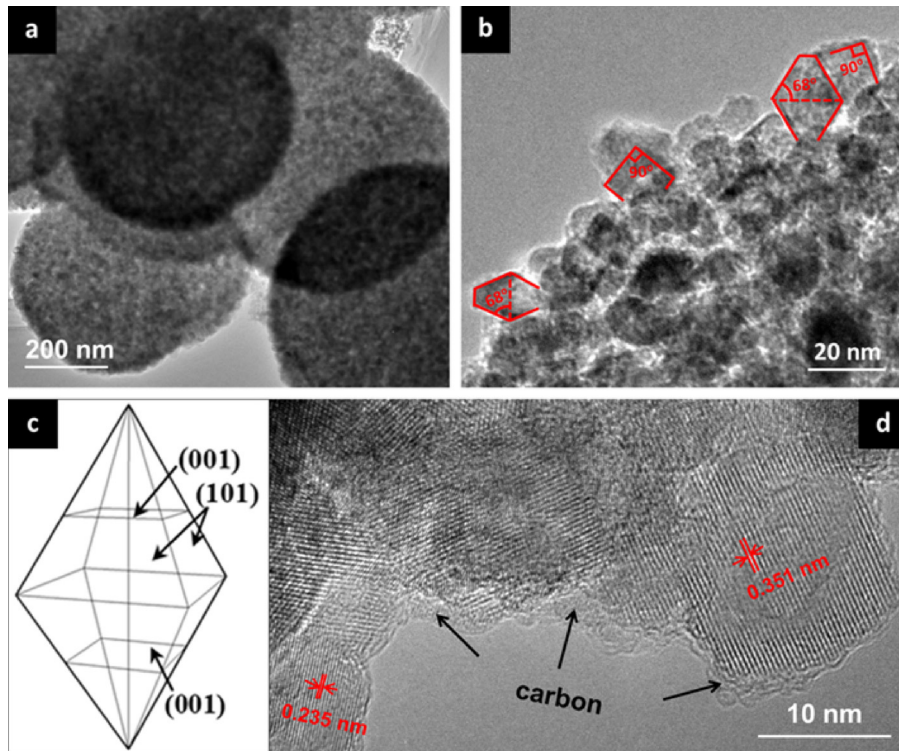
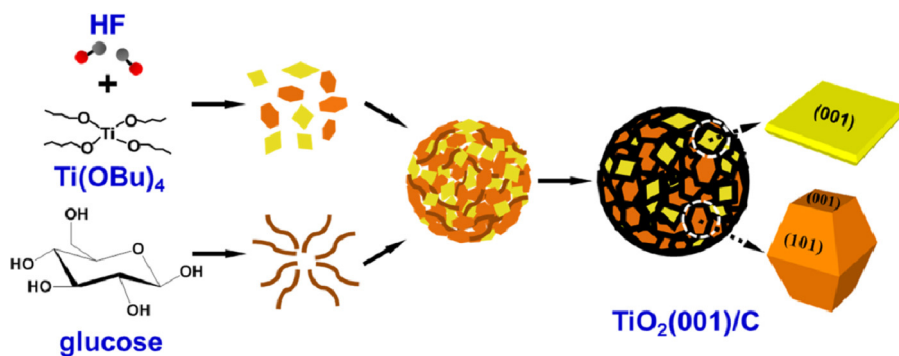


Fig. 2. (a) Low-magnification TEM image of the mesoporous $\text{TiO}_2(001)/\text{C}$ spheres. (b) high-magnification TEM image of a $\text{TiO}_2(001)/\text{C}$ sphere. (c) 3D model of anatase TiO_2 crystal. (d) HRTEM image of the TiO_2 nanocrystals coated with carbon in the spheres.



Scheme 1. Glucose and HF-mediated transformation pathway for the fabrication of $\text{TiO}_2(001)/\text{C}$ microspheres consisting of TiO_2 nanocrystals with exposed $\{001\}$ facets.

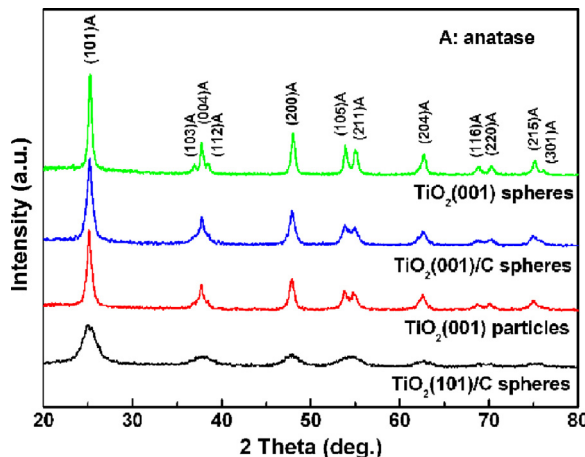


Fig. 3. XRD patterns of TiO_2 samples from hydrothermal reaction.

Based on the Debye–Scherer equation, Table S1 summarizes the average crystallite size of the TiO_2 nanoparticles resulted from different experimental parameters. The crystallite size of TiO_2 grown in the absence of HF is smaller (8.41 nm) compared with that of TiO_2 derived in the presence of HF, which indicates that HF enhances the crystallization of anatase phase and promotes the growth of crystallites [48,49]. After calcination of $\text{TiO}_2(001)/\text{C}$ spheres at 550 °C for 5 h, the peaks of the resultant TiO_2 spheres appear sharper and the crystallite size grow from 13.28 nm to 18.72 nm.

3.2. Surface area and pore distribution

N_2 adsorption–desorption isotherms and the related pore diameter distribution plots were performed for the prepared four TiO_2 samples to further elucidate their porous structure and morphological evolution. As shown in Fig. 4a, all of the four samples exhibit a type IV adsorption with a H1 hysteresis loop, typical for mesoporous materials. The physical properties of these TiO_2 samples are summarized in Table 1. Clearly, both of the BET surface area and pore volume are improved for carbon-containing TiO_2 spheres ($\text{TiO}_2(101)/\text{C}$, and $\text{TiO}_2(001)/\text{C}$) compared to that of TiO_2 particles. However, after calcination of $\text{TiO}_2(001)/\text{C}$ spheres at 550 °C

for 5 h, the BET surface of $\text{TiO}_2(001)/\text{C}$ spheres decreased from $113.3 \text{ m}^2 \text{ g}^{-1}$ to $77.2 \text{ m}^2 \text{ g}^{-1}$, without the apparent change of pore volume. This is possibly ascribed to the removal of carbon species during the calcination process. The pore size distribution calculated from the desorption branch of the nitrogen isotherm by the BJH (Barrett–Joyner–Halenda) method was shown in Fig. 4b. Compared with $\text{TiO}_2(001)$ particles, which present a narrow pore size range of 3.0–10.0 nm with a maximum pore diameter of about 8.9 nm, both $\text{TiO}_2(101)/\text{C}$ spheres and $\text{TiO}_2(001)/\text{C}$ spheres show a peak in the small mesoporous range (about 3.6 nm). While for $\text{TiO}_2(001)$ spheres obtained by calcination of $\text{TiO}_2(001)/\text{C}$ spheres at 550 °C in air, the first peak at about 3.6 nm disappears and the average pore size shift from 11.9 nm to 15.4 nm. We can conclude that the carbon layer in the carbon– TiO_2 composite play an important role in the construction of small mesopores which disappears almost completely upon removal of carbon by pyrolysis/oxidation [50].

3.3. TG Analysis

The amount of carbon content in the carbon-containing TiO_2 microspheres ($\text{TiO}_2(101)/\text{C}$ and $\text{TiO}_2(001)/\text{C}$) are estimated by using thermo-gravimetric (TG) analysis as depicted in Fig. 5a. There are two weight loss regions existing for the two samples. The slight weight loss before 150 °C was attributed to the release of the physically adsorbed water, and the later rapid loss after 200 °C could be attributed to the decomposition of carbonaceous compounds observed by hydrothermal carbonization of glucose which reveals that the amount of carbon in $\text{TiO}_2(101)/\text{C}$ spheres and $\text{TiO}_2(001)/\text{C}$ spheres are about 34.4% and 27.7%, respectively. Obviously, the DTG results (Fig. 5b) indicate that the removal of carbonaceous species in $\text{TiO}_2(101)/\text{C}$ spheres is much easier compared to that of $\text{TiO}_2(001)/\text{C}$, indicating the presence of HF in the hydrothermal system affects not only the exposed facets of TiO_2 nanocrystals but also the composition and structure of the carbonaceous materials further evidenced by the pore structure characterization mentioned above. The removal of the carbon species taking place at low temperature indicates that most of the carbonaceous materials coating on the surface of TiO_2 rather than doping into the TiO_2 lattice [30].

3.4. The chemical states of C, O, F and Ti in $\text{TiO}_2(101)/\text{C}$ and $\text{TiO}_2(001)/\text{C}$ spheres

In order to reveal the chemical states of C, O, and Ti in the carbon-containing TiO_2 microspheres ($\text{TiO}_2(001)/\text{C}$ and $\text{TiO}_2(101)/\text{C}$), these samples were examined with XPS and FTIR. XPS survey spectrum (Fig. S3) show that C, Ti, and O elements exist in $\text{TiO}_2(001)/\text{C}$ and $\text{TiO}_2(101)/\text{C}$ microspheres, and the binding energies for C 1s, Ti 2p3/2 and O 1s are 284.3, 458.5 and 530.4 eV, respectively.

Table 1

Textural property of different TiO_2 samples.

Sample	S_{BET} ($\text{m}^2 \text{ g}^{-1}$)	V_{BJH} ($\text{cm}^3 \text{ g}^{-1}$)	Pore diameter (nm)
$\text{TiO}_2(101)/\text{C}$ spheres	245.8	0.30	3.6
$\text{TiO}_2(001)$ particles	103.8	0.25	8.9
$\text{TiO}_2(001)/\text{C}$ spheres	113.3	0.34	11.9
$\text{TiO}_2(001)$ spheres	77.2	0.33	15.4

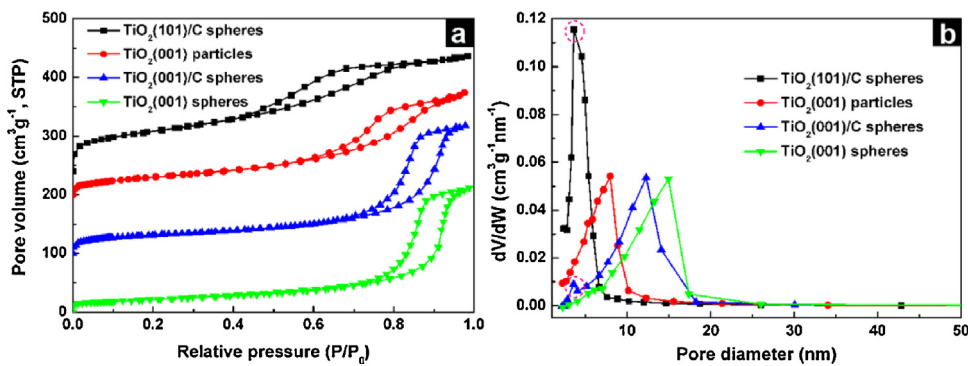


Fig. 4. (a) N₂ adsorption isotherms and (b) the pore size distribution curves of different TiO₂ samples.

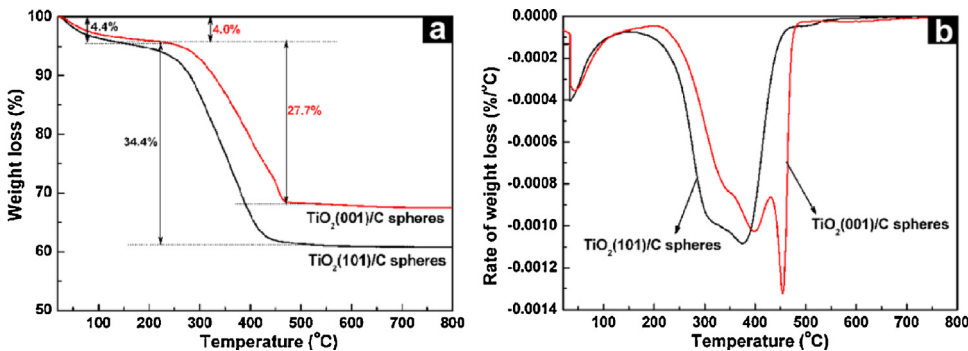


Fig. 5. TG (a) and DTG (b) curves for the TiO₂(001)/C and TiO₂(101)/C spheres.

Fig. 6a shows the C 1s spectral of TiO₂(101)/C and TiO₂(001)/C microspheres, which can be fitted as five peaks at binding energies of 284.6, 285.8, 286.5, 288.4 and 289.2 eV, respectively. The three peaks at 284.6, 285.8 and 286.6 eV are attributed to sp², sp³

hybridized carbon and C–O bond [51] present in TiO₂(001)/C and TiO₂(101)/C spheres, respectively. The peak observed at 288.4 eV is assigned to C–O–Ti bond [52]. The small peak observed around 289.2 eV is also observed on both carbon-containing TiO₂ samples,

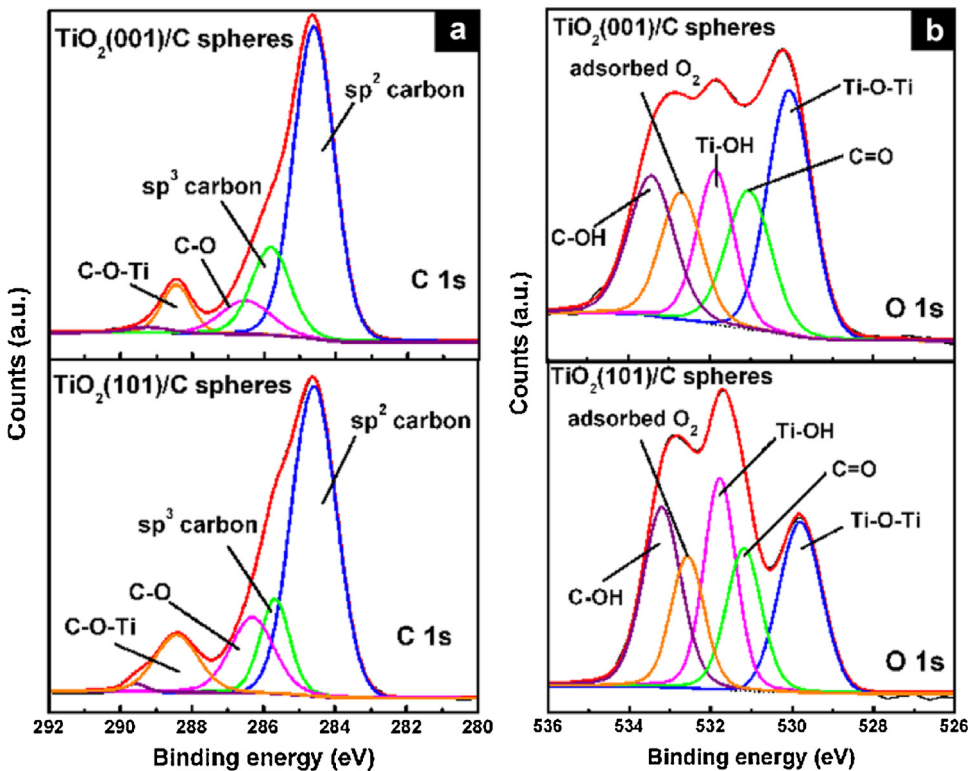


Fig. 6. XPS spectra of survey spectrum (a) C1s and (b) O1s for TiO₂(001)/C and TiO₂(101)/C spheres.

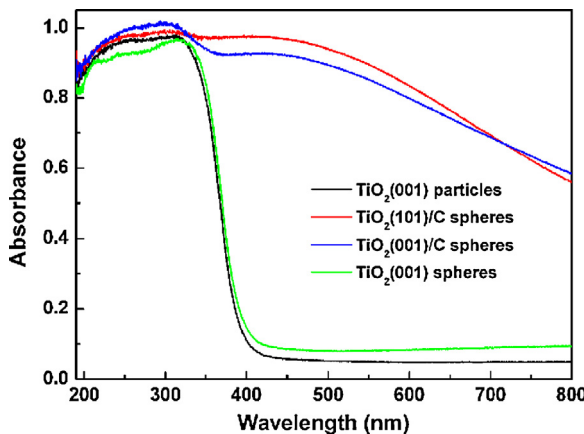


Fig. 7. UV-visible absorbance spectra of different TiO_2 samples.

which could be attributed to carboxyl-containing contamination, mostly likely from adsorbed atmospheric CO_2 [53]. The absence of C 1s peak around 281 eV generally attributed to Ti–C bond excludes the possibility of carbon-doping in TiO_2 lattice [54]. This is different from the results reported in the literature, in which C-doped TiO_2 was also synthesized through the hydrothermal process using glucose as carbon source [55–58]. With respect to the XPS spectra of O1s shown in Fig. 6b, five peaks of 529.8, 531.2, 531.8, 532.7, and 533.4 eV have been fitted, which should be assigned to Ti–O–Ti (lattice oxygen), C=O (and COO), Ti–OH, adsorbed O_2 and C–OH (and C–O–C), respectively [30,59]. It can be inferred that organic carbonaceous materials may form a complex layer around the TiO_2 nanocrystals and combine with the TiO_2 surface via C–O–Ti bonds, which is thought to be favorable for charge transfer upon light excitation [29]. The C–O–Ti bond formation is also explored by FTIR spectroscopy (Fig. S4). For both $\text{TiO}_2(001)/\text{C}$ and $\text{TiO}_2(101)/\text{C}$, the broad absorption at ca. 500 cm^{-1} represents the Ti–O–Ti stretching vibrations, while the bands near 1150 cm^{-1} are assigned to the C–O–Ti stretching modes. The two binding energies of Ti 2p are 458.5 eV (Ti 2p3/2) and 464.2 eV (Ti 2p1/2) as shown in Fig. S5a, which is in good agreement with pure TiO_2 [29,55]. Moreover, high-resolution XPS spectra of the F 1s region in $\text{TiO}_2(001)/\text{C}$ microspheres was also studied as shown in Fig. S5b, the measured binding energy is 684.7 eV, which is a typical value for fluorinated TiO_2 systems, such as $\equiv\text{Ti}-\text{F}$ species on the TiO_2 crystal surface. There are no obvious peaks at 687–689 eV, indicating that F^- anions are not doped into the TiO_2 crystal lattices but present as surface atoms [45,60]. Upon calcination, the peak intensity in $\text{TiO}_2(001)$ spheres was greatly decreased, meaning that the surface adsorbed F^- anions are largely removed. The molar ratio of F/Ti on the surface was decreased from 15.3% to 1.9% as shown in Table S1.

3.5. UV-vis diffuse reflectance spectra analysis

UV-visible diffuse reflectance spectroscopy was used to characterize the electronic states of the as-prepared carbon– TiO_2 composites ($\text{TiO}_2(001)/\text{C}$ spheres and $\text{TiO}_2(101)/\text{C}$ spheres) and pure TiO_2 materials ($\text{TiO}_2(001)$ particles and $\text{TiO}_2(001)$ spheres) as shown in Fig. 7. With respect to the two pure TiO_2 samples, there are no adsorption above their fundamental absorption band edge at about 390 nm, while $\text{TiO}_2(001)/\text{C}$ spheres and $\text{TiO}_2(101)/\text{C}$ spheres exhibit a strong absorption bands from 400 to 800 nm due to the effective photo absorption property of the functional carbonaceous species in the carbon– TiO_2 composites. The carbonaceous materials can introduce a sensitization effect to extend the response of TiO_2 into the visible-light range of the solar spectrum. Moreover, the absorption band edge of $\text{TiO}_2(001)/\text{C}$ composite is red-shift as compared to $\text{TiO}_2(001)$ samples.

3.6. Photocatalytic performances

The decomposition of methyl blue (MB, 10 mg L⁻¹) over carbon-containing TiO_2 ($\text{TiO}_2(001)/\text{C}$ and $\text{TiO}_2(101)/\text{C}$) microspheres under visible light was carried out and compared with that of non-carbon containing TiO_2 ($\text{TiO}_2(001)$ particles and $\text{TiO}_2(001)$ microspheres). Prior to the light irradiation, a preliminary study of MB adsorption was performed using the same amount (0.01 g) of different TiO_2 samples at 20 °C. Fig. S6 shows the kinetics of MB adsorption in the dark during 5 h. For all samples, most of the adsorption was completed within 1 h. The values of MB adsorbed on the carbon– TiO_2 composites ($\text{TiO}_2(001)/\text{C}$ and $\text{TiO}_2(101)/\text{C}$) were much higher than that on $\text{TiO}_2(001)$ particles, and a remarkable loss of adsorption efficiency is observed for $\text{TiO}_2(001)$ spheres after removal of carbon from the hybrid $\text{TiO}_2(001)/\text{C}$ structure. These results indicate that the effective adsorption of MB dye may mainly result from the hydrophobic $\pi-\pi$ interactions between the carbonaceous species on the surface of TiO_2 and the aromatic rings of the dye molecules [61].

The catalytic photo-degradation of MB over different catalysts is investigated. The concentration variation of MB as a function of visible irradiation time for each sample is shown in Fig. 8(a), and the corresponding rate constants in Fig. 8(b). $\text{TiO}_2(001)/\text{C}$ microspheres exhibit the highest degradation efficiency under visible light illumination compared with other catalysts. Obviously, the photocatalytic activity remarkably decreased after the removal of carbon from $\text{TiO}_2(001)/\text{C}$ spheres via calcination at 550 °C for 5 h. Thus, we can conclude that the carbonaceous species deposited onto the surface of TiO_2 nanocrystals could play an optical absorption role to transfer charge from carbon to TiO_2 upon light excitation [31]. Except for the sensitization effect of carbon itself, dye sensitization may also extend the absorption of TiO_2 to

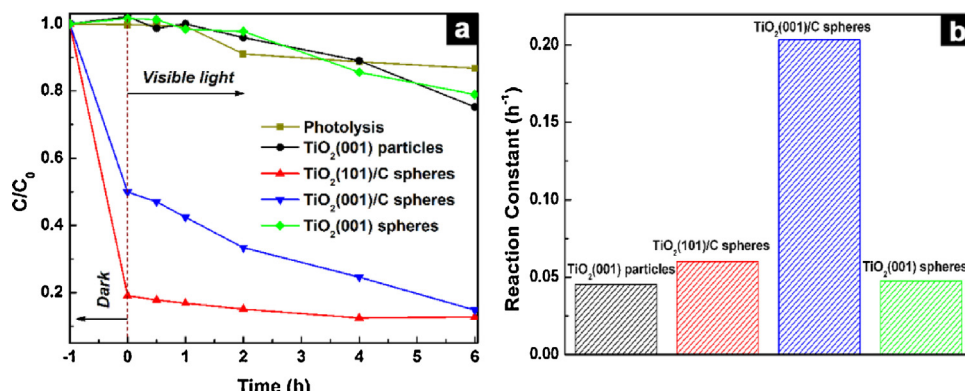


Fig. 8. Degradation profiles of MB (a) and the corresponding reaction constants (b) over different TiO_2 samples under visible light.

visible light region [30,55]. However, the weak degradation of MB over $\text{TiO}_2(001)$ particles and $\text{TiO}_2(001)$ spheres suggests that the photosensitization effect is not the main reason for visible light degradation of MB in the present case. Therefore, it can be concluded that the presence of carbonaceous materials deposited on the TiO_2 nanocrystals is responsible for the photocatalytic activity under visible light irradiation.

The $\text{TiO}_2(001)/\text{C}$ spheres also present higher photocatalytic activity than $\text{TiO}_2(101)/\text{C}$ spheres towards the degradation of MB under UV light, as shown in Fig. S7. Interestingly, the annealing product $\text{TiO}_2(001)$ spheres exhibit much higher activity and reaction constant under UV light irradiation than that of $\text{TiO}_2(001)$ particles, although the specific surface area of $\text{TiO}_2(001)$ particles is nearly 1.4 times higher than that of $\text{TiO}_2(001)$ spheres. It is due to the hierarchical spherical structure and opened porous networks of the synthesized TiO_2 microspheres [45,62]. In addition, $\text{TiO}_2(001)/\text{C}$ spheres show lower activity than that of the corresponding $\text{TiO}_2(001)$ spheres. These results suggest that the carbonaceous species coated on the surface of TiO_2 nanocrystals are not necessary for improving the photocatalytic activity under UV light irradiation, but the hierarchical mesoporous spherical structure and removal of surface-absorbed F^- anions on $\{001\}$ facets may be favorable factors on catalytic activity under UV light.

4. Conclusion

$\text{TiO}_2(001)$ /Chierarchical microspheres assembled from carbon-coated anatase TiO_2 nanocrystals exposed with $\{001\}$ facets were successfully synthesized via a one-step hydrothermal method. The presence of HF promotes the growth of anatase crystal with $\{001\}$ facet exposure, while glucose induces the formation of spherical-like $\text{TiO}_2(001)/\text{C}$ structure and acts as the carbon source during the hydrothermal process. The surface area and mesoporous pore volume were improved after the carbonaceous species deposited on the surface of TiO_2 via C-O-Ti bond, which not only greatly enhance the adsorption ability of dye molecules but also promote the visible light photocatalytic performance for degradation of MB solution. Moreover, such a hierarchical TiO_2 microspheres with exposed reactive $\{001\}$ facets will have potential applications in other fields, such as photo-splitting of water, Li-ion battery and dye-sensitization solar cell.

Acknowledgment

We acknowledge financial supports for this research project from the National Natural Science Foundation of China (grants 51072028, 20876026, 21176043).

Appendix A. Supplementary data

Supplementary data associated with this article can be found, in the online version, at <http://dx.doi.org/10.1016/j.apcatb.2013.10.027>.

References

- [1] A. Fujishima, K. Honda, *Nature* 238 (1972) 37–38.
- [2] M.R. Hoffmann, S.T. Martin, W.Y. Choi, D.W. Bahnemann, *Chem. Rev.* 95 (1995) 69–96.
- [3] C.J. Barbe, F. Arendse, P. Comte, M. Jirousek, F. Lenzmann, V. Shklover, M. Gratzel, *J. Am. Ceram. Soc.* 80 (1997) 3157–3171.
- [4] X. Chen, S.S. Mao, *Chem. Rev.* 107 (2007) 2891–2959.
- [5] T. Ohno, K. Sarukawa, M. Matsumura, *New J. Chem.* 26 (2002) 1167–1170.
- [6] X.Q. Gong, A. Selloni, *J. Phys. Chem. B* 109 (2005) 19560–19562.
- [7] A. Selloni, *Nat. Mater.* 7 (2008) 613–615.
- [8] B.H. Wu, C.Y. Guo, N.F. Zheng, Z.X. Xie, G.D. Stucky, *J. Am. Chem. Soc.* 130 (2008) 17563–17567.
- [9] C.Z. Wen, H.B. Jiang, S.Z. Qiao, H.G. Yang, G.Q. Lu, *J. Mater. Chem.* 21 (2011) 7052–7061.
- [10] U. Diebold, *Surf. Sci. Rep.* 48 (2003) 53–229.
- [11] H.G. Yang, C.H. Sun, S.Z. Qiao, J. Zou, G. Liu, S.C. Smith, H.M. Cheng, G.Q. Lu, *Nature* 453 (2008) 638–641.
- [12] X.G. Han, Q. Kuang, M.S. Jin, Z.X. Xie, L.S. Zheng, *J. Am. Chem. Soc.* 131 (2009) 3152–3153.
- [13] G. Liu, C.H. Sun, H.G. Yang, S.C. Smith, L.Z. Wang, G.Q. Lu, H.M. Cheng, *Chem. Commun.* 46 (2010) 755–757.
- [14] S.W. Liu, J.G. Yu, M. Jaroniec, *Chem. Mater.* 23 (2011) 4085–4093.
- [15] X.H. Yang, Z. Li, G. Liu, J. Xing, C.H. Sun, H.G. Yang, C.Z. Li, *CrystEngComm* 13 (2011) 1378–1383.
- [16] H.G. Yang, G. Liu, S.Z. Qiao, C.H. Sun, Y.G. Jin, S.C. Smith, J. Zou, H.M. Cheng, G.Q. Lu, *J. Am. Chem. Soc.* 131 (2009) 4078–4083.
- [17] G. Liu, H.G. Yang, X.W. Wang, L.N. Cheng, J. Pan, G.Q. Lu, H.M. Cheng, *J. Am. Chem. Soc.* 131 (2009) 12868–12869.
- [18] G. Liu, C.H. Sun, S.C. Smith, L.Z. Wang, G.Q. Lu, H.M. Cheng, *J. Collid Interface Sci.* 349 (2010) 477–483.
- [19] Q.J. Xiang, J.G. Yu, M. Jaroniec, *Phys. Chem. Chem. Phys.* 13 (2011) 4853–4861.
- [20] Q.J. Xiang, J.G. Yu, W.G. Wang, M. Jaroniec, *Chem. Commun.* 47 (2011) 6906–6908.
- [21] J.G. Yu, G.P. Dai, Q.J. Xiang, M. Jaroniec, *J. Mater. Chem.* 21 (2011) 1049–1057.
- [22] X.S. Zhou, F. Peng, H.J. Wang, H. Yu, Y.P. Fang, *Chem. Commun.* 48 (2011) 600–602.
- [23] Z. Xiong, X.S. Zhao, *J. Am. Chem. Soc.* 134 (2012) 5754–5757.
- [24] S.Y. Zhu, S.J. Liang, Q. Gu, L.Y. Xie, J.X. Wang, Z.X. Ding, P. Liu, *Appl. Catal., B* 119 (2012) 146–155.
- [25] D.Q. Zhang, X.L. Yang, J. Zhu, Y. Zhang, P. Zhang, G.S. Li, *J. Sol-Gel Sci. Technol.* 58 (2011) 594–601.
- [26] L.F. Qi, J.G. Yu, M. Jaroniec, *Phys. Chem. Chem. Phys.* 13 (2011) 8915–8923.
- [27] J.G. Hou, C. Yang, Z. Wang, S.Q. Jiao, H.M. Zhu, *Appl. Catal., B* 129 (2013) 333–341.
- [28] C. Lettmann, K. Hildenbrand, H. Kisch, W. Macyk, W.F. Maier, *Appl. Catal., B* 32 (2001) 215–227.
- [29] L. Zhao, X.F. Chen, X.C. Wang, Y.J. Zhang, W. Wei, Y.H. Sun, M. Antonietti, M.M. Titirici, *Adv. Mater.* 22 (2010) 3317–3321.
- [30] J. Zhong, F. Chen, J.L. Zhang, *J. Phys. Chem. C* 114 (2010) 933–939.
- [31] P. Zhang, C.L. Shao, Z.Y. Zhang, M.Y. Zhang, J.B. Mu, Z.C. Guo, Y.C. Liu, *Nanoscale* 3 (2011) 2943–2949.
- [32] M. Inagaki, *Carbon* 50 (2012) 3247–3266.
- [33] X.C. Jiang, T. Herricks, Y.N. Xia, *Adv. Mater.* 15 (2003) 1205–1209.
- [34] H.X. Li, Z.F. Bian, J. Zhu, D.Q. Zhang, G.S. Li, Y.N. Huo, H. Li, Y.F. Lu, *J. Am. Chem. Soc.* 129 (2007) 8406–8407.
- [35] X.L. Bai, B. Xie, N. Pan, X.P. Wang, H.Q. Wang, *J. Solid State Chem.* 181 (2008) 450–456.
- [36] H.J. Koo, Y.J. Kim, Y.H. Lee, W.I. Lee, K. Kim, N.G. Park, *Adv. Mater.* 20 (2008) 195–199.
- [37] H.K. Yu, G.R. Yi, J.H. Kang, Y.S. Cho, V.N. Manoharan, D.J. Pine, S.M. Yang, *Chem. Mater.* 20 (2008) 2704–2710.
- [38] D.H. Chen, L. Cao, F.Z. Huang, P. Imperia, Y.B. Cheng, R.A. Caruso, *J. Am. Chem. Soc.* 132 (2010) 4438–4444.
- [39] W.G. Yang, F.R. Wan, Q.W. Chen, J.J. Li, D.S. Xu, *J. Mater. Chem.* 20 (2010) 2870–2876.
- [40] Z.K. Zheng, B.B. Huang, X.Y. Qin, X.Y. Zhang, Y. Dai, M.H. Jiang, P. Wang, M.H. Whangbo, *Chem. Eur. J.* 15 (2009) 12576–12579.
- [41] S.W. Liu, J.G. Yu, M. Jaroniec, *J. Am. Chem. Soc.* 132 (2010) 11914–11916.
- [42] J.G. Yu, Q.J. Xiang, J.R. Ran, S. Mann, *CrystEngComm* 12 (2010) 872–879.
- [43] F.L. Cao, J.G. Wang, F.J. Lv, D.Q. Zhang, Y.N. Huo, G.S. Li, H.X. Li, J. Zhu, *Catal. Commun.* 12 (2011) 946–950.
- [44] W.G. Yang, J.M. Li, Y.L. Wang, F. Zhu, W.M. Shi, F.R. Wan, D.S. Xu, *Chem. Commun.* 47 (2011) 1809–1811.
- [45] Z.K. Zheng, B.B. Huang, J.B. Lu, X.Y. Qin, X.Y. Zhang, Y. Dai, *Chem. Eur. J.* 17 (2011) 15032–15038.
- [46] X.M. Sun, Y.D. Li, *Angew. Chem. Int. Ed.* 43 (2004) 597–601.
- [47] L. Pan, J. Zou, S. Wang, X. Liu, X. Zhang, L. Wang, *ACS Appl. Mat. Interfaces* 4 (2012) 1650–1655.
- [48] Z. Wang, K. Lv, G. Wang, K. Deng, D. Tang, *Appl. Catal., B* 100 (2010) 378–385.
- [49] Q.J. Xiang, K.L. Lv, J.G. Yu, *Appl. Catal., B* 96 (2010) 557–564.
- [50] J. Matos, A. Garcia, L. Zhao, M.M. Titirici, *Appl. Catal., A* 390 (2010) 175–182.
- [51] A. Ermolieff, A. Chabli, F. Pierre, G. Rolland, D. Rouchon, C. Vannuffel, C. Vergnaud, J. Baylet, M.N. Semeria, *Surf. Interface Anal.* 31 (2001) 185–190.
- [52] L. Chen, F. Chen, Y. Shi, J. Zhang, *J. Phys. Chem. C* 116 (2012) 8579–8586.
- [53] R. Franking, R.J. Hamers, *J. Phys. Chem. C* 115 (2011) 17102–17110.
- [54] H. Irie, Y. Watanabe, K. Hashimoto, *Chem. Lett.* 32 (2003) 772–773.
- [55] W.J. Ren, Z.H. Ai, F.L. Jia, L.Z. Zhang, X.X. Fan, Z.G. Zou, *Appl. Catal., B* 69 (2007) 138–144.
- [56] F. Dong, H.Q. Wang, Z.B. Wu, *J. Phys. Chem. C* 113 (2009) 16717–16723.
- [57] H.Q. Wang, Z.B. Wu, Y. Liu, *J. Phys. Chem. C* 113 (2009) 13317–13324.
- [58] M.Y. Xing, D.Y. Qi, J.L. Zhang, F. Chen, *Chem. Eur. J.* 17 (2011) 11432–11436.
- [59] P. Zhang, C.L. Shao, Z.Y. Zhang, M.Y. Zhang, J.B. Mu, Z.C. Guo, Y.Y. Sun, Y.C. Liu, *J. Mater. Chem.* 21 (2011) 17746–17753.
- [60] J.H. Pan, Z. Cai, Y. Yu, X.S. Zhao, *J. Mater. Chem.* 21 (2011) 11430–11438.
- [61] Y.C. Hsu, H.C. Lin, C.W. Lue, Y.T. Liao, C.M. Yang, *Appl. Catal., B* 89 (2009) 309–314.
- [62] Q.J. Xiang, J.G. Yu, *Chin. J. Catal.* 32 (2011) 525–531.